

# EVOLIN Benchmark: Evaluation of Line Detection and Association

Kirill Ivanov<sup>1,2</sup> Gonzalo Ferrer<sup>1</sup> Anastasiia Kornilova<sup>1</sup>

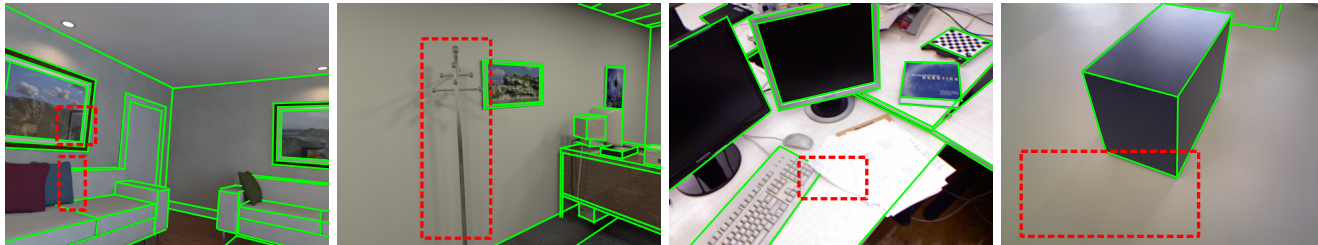


Fig. 1: Examples of annotated lines (green) in ICL NUIM and TUM RGBD datasets from our benchmark. Red indicates elements that were not annotated: reflections, elements that form lines from a certain angle, and shadows.

**Abstract**—Lines are interesting geometrical features commonly seen in indoor and urban environments. There is missing a complete benchmark where one can evaluate lines from a sequential stream of images in all its stages: Line detection, Line Association and Pose error. To do so, we present a complete and exhaustive benchmark for visual lines in a SLAM front-end, both for RGB and RGBD, by providing a plethora of complementary metrics. We have also labeled data from well-known SLAM datasets in order to have all in one poses and accurately annotated lines. In particular, we have evaluated 17 line detection algorithms, 5 line associations methods and the resultant pose error for aligning a pair of frames with several combinations of detector-association. We have packaged all methods and evaluations metrics and made them publicly available on web-page<sup>3</sup>.

## I. INTRODUCTION

Landmark recognition is an essential part of many computer vision algorithms. Thus, the critical task of the Simultaneous Localization and Mapping (SLAM) systems front-end part is the detection of landmarks and their association in a frame stream. In such algorithms, it is popular to use key points as landmarks due to the ease of their recognition. At the same time, point-based SLAM pipelines can produce inaccurate results in poorly textured environments [1], [2]. Such environments, however, often contain many lines, which can significantly increase the accuracy and stability of the autonomous system’s motion trajectory estimation; therefore, lines have recently been actively used in SLAM.

Currently, most line-based SLAM frameworks [1]–[12] use the LSD [13] algorithm or its modifications for detection and LBD [14] or its variations for association. Their popularity can be explained in terms of their speed. At the same time, many detectors [15]–[31] and associations [32]–[41]

have appeared in recent years, including neural networks, which, however, are not actively used in SLAM systems.

The choice of optimal algorithms for use in the SLAM system is problematic, primarily due to the lack of a universal basis for assessing the quality of detection and association, including testing them on famous SLAM sequences. Also, algorithms are often evaluated on data not initially intended for SLAM systems.

This paper provides a universal framework for benchmarking line detection and association algorithms in the SLAM problem. It includes a dataset containing line-annotated images based on known SLAM sequences and metrics for evaluating detection and association algorithms, including line-based relative pose estimation metrics. In addition, we provide a detailed evaluation of popular line detection and association algorithms. Overall, our main contribution is as following.

- Labeled dataset with lines on popular SLAM sequences.
- Set of docker containers with available detection and association algorithms for lines.
- Python library with metrics for detection, association and pose estimation.
- Accuracy and performance evaluation of existing approaches to detection and association on labeled sequences.

## II. RELATED WORK

In our literature review, we tackle the next topics related to line usage in odometry and SLAM pipelines: detection and association algorithms approaches to use lines in SLAM pipelines, popular metrics, and available datasets with lines.

**Line Detectors.** The following classification can be distinguished [42]: (i) approaches based on the Hough transform, (ii) local approach, (iii) combined approach, and (iv) neural network approaches.

*The Hough transform* [43] consists of the transition from the image space to the parameter space and the subsequent search for extreme values corresponding to lines using the

<sup>1</sup>The authors with the Skolkovo Institute of Science and Technology (Skoltech), Center for AI Technology (CAIT). k.ivanov, g.ferrer, anastasiia.kornilova@skoltech.ru

<sup>2</sup>The authors are with the Software Engineering Department, Saint Petersburg State University.

<sup>3</sup><https://prime-slam.github.io/evolin/>

voting procedure. Along with the classical Hough transform [44], there are a large number of optimizations that include probabilistic algorithms [45]–[47], as well as algorithms that analyze neighborhoods of peak values in the parametric space [48].

Algorithms of the *bottom-up approach*, also known as the local approach, exploit the next strategy: first, a primary set of small linear segments are segmented, then they are iteratively linked into larger ones based on the analysis of neighboring elements, optionally having last step to filter our false segments. As the authors of the work [13] showed, early detectors [49], [50] performed slowly and recognized many insignificant line segments. In subsequent works, the mechanisms for controlling false alarms have been optimized [13], [18], and a significant acceleration of the detectors is achieved [15], [19].

*Combined approach* algorithms use information obtained from the input image and the parametric Hough transform space, which accelerates the voting process [51], selects likely candidates for the local approach [52], and filters false positives [17].

Thanks to the development of deep learning in the last decade, multiple *neural network algorithms* have appeared for detecting line segments. Various methods have been proposed for recognizing line segments in images, such as extracting them from attraction field maps [21] and point-pair graph-based detection [23]. Different architectures have been proposed for line detection, such as transformer-based [27], fully convolutional [31], and having a trainable module that performs the Hough transform [24]. Various line representations have also been proposed, such as tri-point [25] and Bezier curves [29]. In addition, real-time detectors have been proposed [28], [30]. The wireframe parsing problem is also formulated [20], [22], [26], consisting of finding a set of segments in the image and their junctions.

**Line Association.** The following approaches can be distinguished [53]: (i) line descriptor, (ii) a junction-based approach, (iii) invariants between lines and points, (iv) line segment grouping, and (v) neural networks.

A *line segment descriptor* is usually represented as a fixed-dimensional vector. An association between segments is established if the distance between the corresponding descriptors is less than a given threshold. In early works [54], [55], this approach was used to construct association algorithms, while the descriptor could include information about the gradient, intensity, and color in the neighborhood of the lines. In subsequent works [14], [56], [57], optimizations are applied to ensure the resilience of descriptors to changes in lighting and scale.

*Junction-based association* matches segments in pairs based on their intersection points. Thus, in [58], the authors use the coplanarity of pairs of intersecting lines to separate true matches from false ones. In [32], a ray-point-ray descriptor is proposed, aggregating information about the lines and their intersection point. The authors of the work [33] propose a hierarchical two-stage algorithm that matches line-junction-line descriptors at the first stage and descriptors of

individual lines at the second.

*Line association using invariants between coplanar points and line segments* [34], [59] usually establishes correspondences between points by well-known algorithms. After that, line segments that satisfy the invariants are considered true matches.

*Algorithms using the grouping approach* are based on creating groups of line segments according to some criterion with their subsequent comparison. Thus, it is proposed to form groups of linear segments lying next to each other based on the similarity of the average gradient values of all pixels of the segments [60]. The authors of work [39] propose dividing all detected line segments into three hierarchical groups and then establishing correspondences sequentially for each group using information obtained from the associations of the previous group.

In recent years, *neural-based* association has also appeared in addition to detectors. In such algorithms, neural network architectures based on convolutional layers are the most popular [35]–[37]. Lines can also be represented as sequences of points, allowing techniques from natural language processing [40] and point association [61] to be applied.

**Line-based SLAM.** In the last years, a set of SLAM algorithms that exploit lines in graph optimizations have been presented by the community [1]–[4], [7], [9]–[11], [62]–[64]. They can be categorized by approaches used in SLAM front-end and back-end. The common choice for SLAM front-end, namely for detection and association, is LSD detector [13] and LBD association [14]. Back-end approaches can be differed by the way of line representation and observation function. The most commonly used representations are Plucker coordinates and line end points. Using this, different variations of observation functions are provided based on reprojection error: end points error, point-to-line error.

**Datasets.** Two widely used datasets for line detection evaluation — YorkUrban [65] and ShanghaiTech Wireframe [20]. They contain accurate annotations for lines but do not provide sequential frames, making them difficult to apply to the line association problem. In order to test line association, several approaches are used, such as projective transformations of original images [41], [61], automatic annotation [36], [40], or referenceless comparison on successive frames [35].

**Metrics.** Line segments can be represented in vector form, i.e., endpoints, and raster form, in the form of a set of points, making it possible to evaluate two types of detection metrics. In the vector case, one can evaluate *the structural average precision (sAP)* and *the structural F-score* [22], [24], [26], [27]. Also, in work [61], repeatability metrics are proposed that reflect the proportion of the same lines detected on different frames. In the raster case, it is possible to calculate the average heatmap precision ( $AP^H$ ) and heatmap F-score ( $F^H$ ) [20], [66]. Like detection, line association can be viewed as a classification task [36], [37], [61] based on which known metrics such as *precision*, *recall*, *F-score*, and others are applied. In addition, it is possible to evaluate the performance of association using metrics for visual localization and homography estimation [40] and, by

integrating into the SLAM pipeline, to evaluate the resulting trajectory [35].

### III. DATA ANNOTATION

Existing datasets with lines [20], [65] do not provide a labeled frame stream with line labels and associations that is required for SLAM evaluation (front-end and back-end). This section describes the choice of datasets for annotating lines within our benchmark and the annotating process.

#### A. Dataset Choice

Popular datasets for evaluating line detectors and association do not contain consecutive frames, which makes it difficult to assess their applicability in SLAM pipelines. To solve this problem, we choose the ICL-NUIM [67] and TUM RGB-D [68] datasets for line segment annotation, which contain consecutive frames and are actively used to evaluate the performance of SLAM systems. The choice of these datasets is also due to the fact that they are already annotated with planes [69], which allows the creation of a joint framework for testing lines, points, and planes in the front-end of SLAM. We take trajectories `lr kt2` and `of kt2` from ICL NUIM that scan the whole scene, and trajectories `fr3/cabinet` and `fr1/desk` from TUM RGB-D for annotating.

#### B. Annotation process

The above-specified datasets are annotated manually using the CVAT tool [70], which allows tracking lines on successive frames, which is important for obtaining ground truth associations. The annotation process consisted of the following steps: defining lines on the first frame, interpolating lines on subsequent frames using the CVAT functionality, and correcting lines on intermediate frames. If the line is absent on the scene, it is not displayed in the track on the corresponding frames. Only breaking segments have been annotated, such as ceilings, floors, walls, doors, and furniture linear elements. Examples of different scene annotations can be seen in Fig. 1. Linear locally and texture elements are not annotated. The statistics of annotated lines among labeled datasets are presented in Tab. I.

TABLE I: Statistics on annotated line segments on selected datasets

Dataset	# lines	# frames	Lines per Frame
lr kt2	189	881	47
of kt2	346	881	78
fr3/cabinet	46	1147	13
fr1/desk	184	613	51

### IV. METRICS

This section describes the detection and association metrics used in our benchmark and the relative pose estimation metrics based on line correspondences. We combine them into a single Python-library.

#### A. Detection

One can distinguish between *vectorized* and *heatmap-based* metrics depending on the line representation. In the first, line segments are defined by their endpoints, and in the second, by rasterized points.

**Vectorized metrics** include adapted versions of classification [22] and repeatability [61] metrics. Both groups of metrics require a distance function  $d(l_1, l_2)$ , where  $l_i = (p_i^1, p_i^2)$  is an  $i$ -th line segment defined by its endpoints  $p_i^1, p_i^2 \in \mathbb{R}^2$ . As in work [61], we use the following distances.

Structural distance between lines  $i$  and  $j$ :

$$d_s(l_i, l_j) = \min\{\|p_j^1 - p_i^1\|_2 + \|p_j^2 - p_i^2\|_2, \|p_j^1 - p_i^2\|_2 + \|p_j^2 - p_i^1\|_2\}. \quad (1)$$

Orthogonal distance between lines  $i$  and  $j$ :

$$d_\perp(l_i, l_j) = \frac{d_a(l_i, l_j) + d_a(l_j, l_i)}{2}, \quad (2)$$

where

$$d_a(l_i, l_j) = \|p_j^1 - \pi_{l_i}(p_j^1)\|_2 + \|p_j^2 - \pi_{l_i}(p_j^2)\|_2, \quad (3)$$

and  $\pi_l(\cdot)$  is the orthogonal projection onto the line  $l$ .

a) *Classification metrics*: A detected line segment  $l_j$  is considered True Positive (TP) if and only if the following conditions are met:

- $\min_{l \in GT} d(l_j, l) \leq d_{max}$ , where  $d_{max}$  is the maximum allowable distance between the predicted and reference segments expressed in pixels, and  $GT$  is the set of ground truth line segments;
- if there exists  $l_i$  such that  $\arg \min_{l \in GT} d(l_i, l) = l'$ , then  $l_j$  must have a higher detector confidence level than  $l_i$  in case the detector provides confidence values for each segment. If the detector does not provide such values, then the inequality  $d(l_j, l') < d(l_i, l')$  must hold.

After establishing for each predicted line whether it is TP or False Positive (FP), we can calculate classical classification metrics such as *precision*, *recall*, *F-score*, and *average precision*.

b) *Repeatability metrics*: Since the annotated datasets contain information about the depth and intrinsic camera parameters, we explicitly reproject lines from one frame to another rather than using synthetic homographies, as in work [61]. Let  $L_1$  and  $L_2$  be the sets of lines in the first and second images, respectively, and  $P_{i \rightarrow j}(\cdot)$  be the transformation mapping the lines from the  $i$ -th image to the  $j$ -th. Let  $L'_1 = P_{1 \rightarrow 2}(L_1)$  and  $L'_2 = P_{2 \rightarrow 1}(L_2)$ . We also need to define the following indicator that the distance from the line  $l$  to the set of lines  $L$  is less than the threshold  $d_{max}$ :

$$I_L(l) = \begin{cases} 1, & \text{if } \min_{l_j \in L} d(l, l_j) \leq d_{max} \\ 0, & \text{otherwise} \end{cases}, \quad (4)$$

where  $d(\cdot, \cdot)$  is either an orthogonal or structural distance, as described earlier. Now we can define the *repeatability* metric showing the proportion of lines found on both the

first and second frames and the *localization error* — the average distance between such lines.

- Repeatability:

$$\text{Rep-}d_{max} = \frac{\sum_{l_i \in L'_1} I_{L_2}(l_i) + \sum_{l_j \in L'_2} I_{L_1}(l_j)}{|L_1| + |L_2|}. \quad (5)$$

- Localization error: Let  $\text{Dist}(L_j, L_i)$  be the set of closest distances from each line in  $L_j$  to some line in  $L_i$  within the threshold  $d_{max}$ , which is defined as follows:

$$\text{Dist}(L_j, L_i) = \left\{ \min_{l_i \in L_i} d(l_i, l) \mid I_{L_i}(l) = 1, l \in L_j \right\} \quad (6)$$

Then the *localization error* is defined as follows:

$$\text{LE-}d_{max} = \frac{\sum_{d \in \text{Dist}(L_2, L_2) \cup \text{Dist}(L'_1, L_1)} d}{|\text{Dist}(L'_2, L_2)| + |\text{Dist}(L'_1, L_1)|} \quad (7)$$

Here,  $|\cdot|$  is the set cardinality.

**Heatmap-based metrics.** In the case of a raster representation of lines, we consider detection to classify each pixel from the point of view of belonging to any line, as in the works [20], [66]. In this context, a heatmap is a boolean matrix that has the same size as the original image and is obtained by rasterizing the predicted or reference line segments such that each of its elements shows the belonging of the corresponding pixel to any segment. To calculate the metric, it is necessary to build heatmaps of the predicted and reference line segments, then determine which pixels on the predicted heatmap are TP and FP. To do this, it is necessary to solve the minimum weight assignment problem [66], in which the nodes are pixels, and the weights are the distances between them. Only those elements from the predicted heatmap marked as true and the distance from which some reference pixel is less than the specified threshold  $d_{max}$  are included in the consideration. The remaining pixels labeled as true pixels are considered FP. After solving this problem, we have a matrix of indicators, whether the corresponding pixel is TP or not, based on which we can calculate well-known classification metrics.

### B. Association

The problem of finding associations between lines on successive frames can also be considered a classification problem. Given a set of ground truth associations  $GT$ , we can assign each predicted association to one of the following classes: **TP** if it is established and belongs to the  $GT$  set; **FP** if it is established and does not belong to the  $GT$  set; **TN** if it is not established and does not belong to the  $GT$  set; **FN** if it is not established and belongs to the  $GT$  set.

Popular classification metrics are calculated based on the characteristics obtained, as in the case of detection.

### C. Pose estimation error

We also provide a mechanism to evaluate detectors and association quality for pose estimation problem, in similar manner to keypoint detection and association benchmarks [71], [72]. To do this, we formulate optimization problem in the way proposed in work [3]. Let  $P, Q \in \mathbb{R}^3$

be endpoints of line in 3D map,  $p, q \in \mathbb{R}^2$  — its detections on image plane,  $\bar{p}, \bar{q} \in \mathbb{P}^2$  — corresponding homogeneous coordinates. Then we define line observation  $l \in \mathbb{P}^2$  by its coefficients:

$$l = \frac{\bar{p} \times \bar{q}}{|\bar{p} \times \bar{q}|} \quad (8)$$

Then line error could be formulated as:

$$e(T) = \|l^\top \pi(TP)\|^2 + \|l^\top \pi(TQ)\|^2, \quad (9)$$

where  $\pi(\cdot)$  denotes projection of the 3D point to the image plane in homogenous coordinates,  $T \in SE(3)$  describes transformation from the map to the observed frame.

It is worth to note that since our annotated dataset contains depth information, it is easy to calculate 3D points corresponding to line edges. Finally, we estimate relative pose  $T$  by extending g2o framework [73] with an edge implementation that describes this observation function. Also, in optimizations robust Huber kernel was used to filter out outliers as done in majority of existing line-based SLAM. When relative pose is estimated, statistics on translation and rotation error can be calculated.

## V. EXPERIMENTS

This section provides an evaluation of existing line detection and association algorithms on our line-annotated data.

### A. Experimental Settings

**Hardware.** For the evaluations, a machine with the following characteristics was used: 11th Gen Intel(R) Core(TM) i5-11300H @ 3.10GHz, 24 GB RAM, GeForce RTX 3060 Mobile 6 GB.

**Line Detectors.** We have compared and evaluated a total of 17 algorithms: AFM [21], ELSESED [19], F-Clip [31], HAWP [26], HT-LCNN [24], L-CNN [22], LETR [27], LSDNet [30], LSWMS [74], M-LSD [28], TP-LSD [25], ULSD [29], FSG [18], and SOLD2 [61]. Implementations of the following algorithms were taken from OpenCV: LSD [13], EDLines [15], and FLD [16]. All methods are packaged into docker containers.

**Line Association.** For comparison, we select five association algorithms with an open implementation into docker containers: LBD [14], DLD [36], WLD [37], LineTR [40], and SOLD2 [40]. We use brute force matching of descriptors for LBD, DLD, and WLD and matching algorithms proposed by the authors for LineTR and SOLD2.

**Datasets.** For comparison, we use all frames of line-annotated trajectories in `lr kt2`, `of kt2` from ICL NUIM, and `fr3/cabinet`, `fr1/desk` from TUM RGB-D.

### B. Line Detection

Among the metrics built on the vector representation of the line, for algorithms that provide a measure of uncertainty for each line, we choose the average precision ( $AP$ ) for distances  $d_s$  and  $d_\perp$ , from (1) and (2), with a threshold of 5 and 10 pixels and also built PR curves and compared the

TABLE II: Comparison of detectors with line uncertainty measure: average precision for structural ( $sAP$ ) and orthogonal ( $oAP$ ) distances with a 5 and 10 pixels threshold and FPS.

Algorithm	lr kt2					of kt2					fr1/desk					fr3/cabinet				
	$sAP^5$	$sAP^{10}$	$oAP^5$	$oAP^{10}$	FPS	$sAP^5$	$sAP^{10}$	$oAP^5$	$oAP^{10}$	FPS	$sAP^5$	$sAP^{10}$	$oAP^5$	$oAP^{10}$	FPS	$sAP^5$	$sAP^{10}$	$oAP^5$	$oAP^{10}$	FPS
AFM	32.2	41.4	54.6	56.8	12	16.0	23.3	42.9	46.2	12	10.4	19.3	28.0	34.3	11	39.0	49.3	66.0	70.7	10
ELSESED	23.2	29.3	47.4	48.6	107	14.7	22.9	40.7	42.0	98	16.0	24.4	38.1	41.1	69	56.0	63.8	76.9	77.8	162
F-Clip	68.6	74.0	79.5	80.0	30	<b>67.5</b>	<b>72.4</b>	<b>75.5</b>	<b>77.2</b>	29	36.3	42.7	46.7	50.5	29	87.1	87.5	90.5	90.9	29
HAWP	<b>73.2</b>	<b>77.8</b>	<b>82.0</b>	<b>82.6</b>	25	66.3	70.9	73.0	75.0	23	36.1	42.1	45.2	49.1	23	87.7	88.8	89.5	90.2	26
HT-LCNN	68.2	73.3	76.8	77.2	7	61.6	65.9	68.4	70.3	6	33.1	39.2	41.6	45.9	5	82.8	83.2	84.2	84.6	8
L-CNN	67.0	72.2	76.0	76.5	17	61.2	66.0	67.7	69.8	11	31.7	37.5	40.0	43.7	8	83.7	84.2	85.3	86.0	25
LETR	64.8	72.2	78.9	79.6	8	60.5	69.5	72.3	74.4	8	<b>38.3</b>	<b>49.1</b>	<b>54.0</b>	<b>58.9</b>	8	87.0	88.8	91.1	91.7	8
LSD	17.3	23.1	44.8	46.3	111	12.8	19.9	41.6	43.7	112	8.3	16.7	31.5	35.6	61	30.9	39.8	60.0	61.6	139
LSDNet	33.3	42.5	54.4	55.7	13	13.0	19.5	36.2	39.7	13	12.7	22.7	31.8	37.1	13	54.0	60.3	74.4	75.9	13
LSWMS	1.5	3.9	10.7	14.6	20	2.9	8.2	20.5	27.7	25	1.5	5.2	11.1	17.3	20	1.8	3.3	10.3	14.2	19
M-LSD	60.3	67.8	74.4	75.3	98	51.9	58.3	65.5	68.5	103	33.9	40.8	44.7	48.8	99	84.8	86.1	89.4	89.9	111
TP-LSD	70.1	77.5	81.6	82.2	17	58.1	64.5	68.2	70.4	17	35.3	41.7	44.8	48.5	17	<b>88.1</b>	<b>89.0</b>	<b>91.2</b>	<b>91.7</b>	17
ULSD	71.4	76.4	79.6	80.1	27	62.5	67.3	70.9	72.3	26	34.1	40.4	43.4	47.3	25	87.6	88.9	89.4	90.3	28

TABLE III: Comparison of detectors without line uncertainty measure: precision ( $P$ ), recall ( $R$ ), and F-score ( $F$ ) for structural and orthogonal distances with a 5 pixels threshold and FPS.

Algorithm	lr kt2					of kt2					fr1/desk					fr3/cabinet												
	$d_s$			$d_{\perp}$		FPS	$d_s$			$d_{\perp}$		FPS	$d_s$			$d_{\perp}$		FPS	$d_s$			$d_{\perp}$		FPS				
	$P^5$	$R^5$	$F^5$	$P^5$	$R^5$		$F^5$	$P^5$	$R^5$	$F^5$	$P^5$		$R^5$	$F^5$	$P^5$	$R^5$	$F^5$		$P^5$	$R^5$	$F^5$	$P^5$	$R^5$		$F^5$			
EDLines	12.1	56.2	19.9	19.2	89.0	31.6	387	14.7	50.8	22.8	24.0	82.5	37.1	325	4.2	50.9	7.8	7.7	93.2	14.3	213	12.9	68.0	21.7	18.0	94.5	30.2	679
FLD	10.5	45.6	17.0	18.9	82.3	30.7	346	13.1	45.7	20.4	22.7	79.1	35.3	284	4.0	42.9	7.3	8.3	89.9	15.2	180	13.4	54.6	21.5	21.9	89.2	35.2	668
FSG	28.8	43.4	34.6	42.1	63.4	50.6	39	26.7	28.0	27.3	51.5	54.0	52.7	38	11.0	41.6	17.4	19.3	73.0	30.5	21	38.7	63.4	48.0	50.1	82.2	62.3	51
SOLD	8.8	24.7	13.0	23.7	66.5	35.0	3	11.5	27.4	16.2	24.9	59.3	35.1	3	6.5	9.3	7.7	22.4	32.3	26.5	4	26.5	42.8	32.8	40.0	64.5	49.4	7

rest of the algorithms using precision, recall, and F-score. We scale the lines to the  $128 \times 128$  resolution to reduce the impact of image resolution. Among the heatmap-based metrics, we have taken average precision and PR curves for algorithms that measure line uncertainty and precision, recall, and F-score for the rest of the algorithms. We also compute the repeatability metrics for the previously specified distances with a threshold of 5 pixels on the datasets. These metrics are not calculated on the TUM fr1/desk due to the poor quality of the depth maps. In this case, we filter the line segments output by the detector with the threshold of the uncertainty measure if it is available.

The results of the detectors comparison are provided in tables II to VI and in fig. 2. It can be seen that many detectors based on neural networks, such as HAWP, F-Clip, and LETR, have similar results and significantly outperform hand-crafted algorithms, such as LSD and ELSESED, on vectorized and heatmap metrics. At the same time, hand-crafted algorithms show excellent results on repeatability metrics, probably because the line segments detected by neural networks are often displaced relative to the actual lines, as seen in fig. 3, which leads to incorrect reprojection.

### C. Line Association

For association comparison, we use our line annotations and the following metrics: precision, recall, and F-score. Comparison of results are presented in table VII. It is noticeable that LineTR has the highest precision among the presented algorithms but relatively low recall. SOLD2, in

TABLE IV: Comparison of detectors with a lines uncertainty measure: average heatmap precision ( $AP^H$ ) and heatmap F-score ( $F^H$ ).

Algorithm	lr kt2		of kt2		fr1/desk		fr3/cabinet	
	$AP^H$	$F^H$	$AP^H$	$F^H$	$AP^H$	$F^H$	$AP^H$	$F^H$
AFM	62.7	75.6	65.1	75.8	64.3	78.0	41.1	55.7
ELSESED	57.1	68.4	52.8	68.0	80.5	82.5	52.2	56.1
F-Clip	86.5	83.0	87.8	81.0	94.8	92.5	59.4	63.0
HAWP	<b>91.7</b>	<b>85.7</b>	<u>89.1</u>	<b>82.1</b>	96.5	92.0	<u>59.6</u>	61.6
HT-LCNN	87.5	82.4	87.2	81.5	91.5	89.3	55.8	60.2
L-CNN	87.1	82.2	87.1	<b>82.1</b>	92.5	89.1	54.3	59.2
LETR	89.6	82.8	<b>89.3</b>	<u>81.7</u>	<u>96.8</u>	<u>93.0</u>	<b>65.7</b>	<b>65.6</b>
LSD	58.0	65.1	45.3	64.3	61.0	61.7	44.3	49.3
LSDNet	77.6	77.8	74.2	80.1	87.3	82.0	54.9	61.0
LSWMS	32.7	57.3	37.6	58.0	39.2	62.8	24.1	46.7
M-LSD	82.7	77.8	79.8	76.3	92.9	88.6	57.4	62.1
TP-LSD	<u>90.2</u>	<u>85.1</u>	85.1	79.3	<b>97.4</b>	<b>93.5</b>	57.2	60.9
ULSD	88.7	84.7	86.2	79.4	95.3	91.0	56.6	60.1

TABLE V: Comparison of detectors without a lines uncertainty measure: heatmap precision ( $P^H$ ), recall ( $R^H$ ), and F-score ( $F^H$ ).

Algorithm	lr kt2			of kt2			fr1/desk			fr3/cabinet		
	$P^H$	$R^H$	$F^H$	$P^H$	$R^H$	$F^H$	$P^H$	$R^H$	$F^H$	$P^H$	$R^H$	$F^H$
EDLines	52.5	<b>86.4</b>	65.3	61.6	<b>78.2</b>	68.9	26.5	<b>91.6</b>	41.1	57.9	<b>93.5</b>	71.5
FLD	53.6	<u>79.3</u>	64.0	60.9	<u>72.6</u>	66.2	28.1	<u>86.4</u>	42.4	<u>66.1</u>	<u>87.6</u>	<u>75.3</u>
FSG	<u>57.4</u>	78.8	<u>66.4</u>	<u>63.6</u>	67.7	65.6	29.6	83.1	<u>43.6</u>	53.0	87.2	65.9
SOLD2	<b>74.5</b>	66.6	<b>70.3</b>	<b>81.1</b>	67.5	<b>73.7</b>	<b>62.9</b>	36.2	<b>45.9</b>	<b>87.0</b>	66.9	<b>75.6</b>

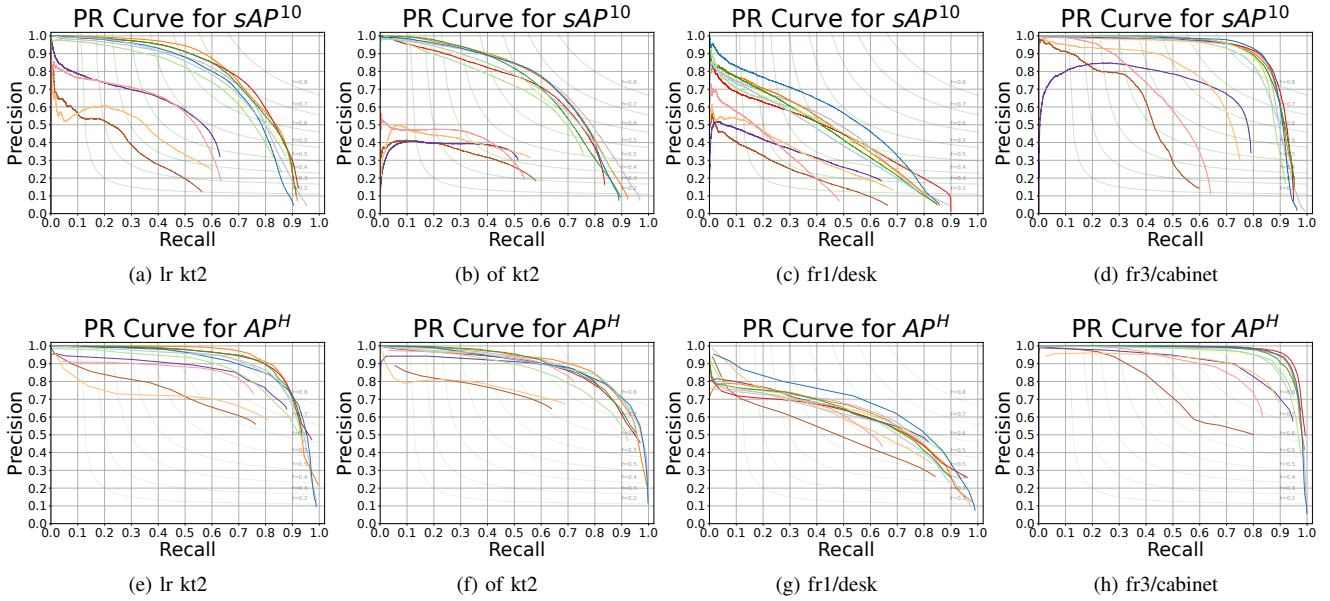


Fig. 2: Precision-Recall curves for  $sAP^{10}$  and  $AP^H$

TABLE VI: Repeatability metrics.

Algorithm	lr kt2				of kt2				fr3/cabinet			
	$d_s$		$d_{\perp}$		$d_s$		$d_{\perp}$		$d_s$		$d_{\perp}$	
	Rep-5 $\uparrow$	Loc-5 $\downarrow$	Rep-5 $\uparrow$	Loc-5 $\downarrow$	Rep-5 $\uparrow$	Loc-5 $\downarrow$	Rep-5 $\uparrow$	Loc-5 $\downarrow$	Rep-5 $\uparrow$	Loc-5 $\downarrow$	Rep-5 $\uparrow$	Loc-5 $\downarrow$
AFM@0.1	0.21	2.48	0.44	1.79	0.19	2.51	0.40	1.66	0.08	2.49	0.24	2.51
ELSED@0	0.33	2.56	0.51	1.43	0.36	2.44	<u>0.52</u>	<b>1.28</b>	0.18	2.91	0.37	1.80
F-Clip@0.4	0.34	2.24	0.53	1.57	0.34	<u>2.06</u>	0.47	1.41	<b>0.27</b>	2.54	0.37	1.91
HAWP@0.8	0.35	<b>2.16</b>	<b>0.55</b>	1.52	0.35	2.11	0.47	1.41	<b>0.27</b>	2.41	0.35	1.82
HT-LCNN@0.98	0.32	<u>2.22</u>	0.51	1.55	0.31	<b>2.01</b>	0.45	1.36	0.23	<b>2.20</b>	0.30	1.75
L-CNN@0.98	0.33	2.27	0.53	1.55	0.31	2.07	0.45	1.40	0.25	2.43	0.33	1.86
LETR@0.7	0.33	2.45	0.53	1.67	0.35	2.44	0.48	1.66	0.30	2.59	0.39	1.92
LSD@0	<b>0.43</b>	2.56	0.52	<b>1.40</b>	<b>0.45</b>	2.41	0.51	1.31	0.21	2.89	0.35	<u>1.73</u>
LSDNet@0.8	0.30	2.44	0.50	1.58	0.30	2.33	0.45	1.41	0.20	2.53	0.34	1.90
LSWMS@0	0.28	3.04	0.41	1.71	0.20	3.19	0.31	2.09	0.16	3.28	0.23	2.16
M-LSD@0.4	0.33	2.42	0.50	1.57	0.35	2.25	0.47	1.51	0.24	2.59	0.32	1.89
TP-LSD@0.3	0.32	2.30	0.52	1.53	0.36	2.21	0.49	1.43	<b>0.27</b>	2.51	0.37	1.89
ULSD@0.9	0.34	2.25	<u>0.54</u>	1.54	0.32	2.09	0.46	1.42	<u>0.26</u>	2.48	0.35	1.85
EDLines	<u>0.40</u>	2.60	0.51	<b>1.40</b>	<u>0.43</u>	2.52	0.51	1.31	<u>0.26</u>	3.00	<b>0.44</b>	1.76
FLD	0.39	2.70	0.51	<u>1.42</u>	<u>0.43</u>	2.58	0.50	<u>1.29</u>	0.21	2.97	<u>0.41</u>	1.83
FSG	0.25	2.53	0.52	1.49	0.27	2.48	<b>0.53</b>	1.44	0.14	2.66	0.34	<b>1.72</b>
SOLD2	0.38	2.59	0.47	1.51	0.42	2.35	0.47	1.33	0.15	<u>2.39</u>	0.28	1.78

turn, outperforms the rest of the algorithms regarding recall and F-score. It is also worth clarifying that LBD also shows quite good results.

#### D. Pose estimation

Relative pose estimations, as described in Sec. IV-C, are derived from the line matches obtained using each association and three popular detectors: LSD, F-Clip, and

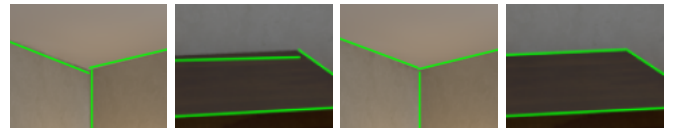


Fig. 3: Detected lines displacement: F-Clip (two images on the left) and LSD (two images on the right).

TABLE VII: Associators comparison: precision ( $P$ ), recall ( $R$ ), F-score ( $F$ ), and FPS

Algorithm	lr kt2				of kt2				fr1/desk				fr3/cabinet			
	P	R	F	FPS	P	R	F	FPS	P	R	F	FPS	P	R	F	FPS
LBD	84.8	69.6	76.4	94	86.0	73.7	79.4	80	36.6	25.2	29.8	109	83.3	50.9	63.2	195
DLD	81.8	64.4	72.1	30	78.3	64.7	70.8	16	23.9	16.3	19.4	23	73.6	49.1	58.9	74
WLD	82.5	66.7	73.8	4	80.3	61.8	69.8	2	35.5	22.7	27.7	3	86.7	63.8	73.5	13
LineTR	96.8	56.7	71.5	14	95.7	61.6	75.0	12	69.5	6.8	12.5	14	96.9	41.2	57.8	19
SOLD2	88.1	80.8	84.3	2	89.2	82.2	85.5	1	42.3	32.4	36.7	2	94.2	84.6	89.1	4

TABLE VIII: Pose error estimation: median translation error and rotation error; a dash means that the pose could not be calculated in more than half of the cases.

Detector	Associator	lr kt2		of kt2		fr3/cabinet	
		$\epsilon_{trans}$	$\epsilon_{rot}$	$\epsilon_{trans}$	$\epsilon_{rot}$	$\epsilon_{trans}$	$\epsilon_{rot}$
LSD	LBD	0.452	7.888	0.446	6.986	1.074	28.052
	DLD	0.206	3.589	0.315	4.585	1.067	32.883
	WLD	0.383	7.259	0.765	13.199	0.818	22.637
	LineTR	<b>0.025</b>	<b>0.890</b>	<b>0.026</b>	<b>0.683</b>	0.620	17.384
	SOLD2	0.144	2.902	0.099	1.917	<b>0.162</b>	<b>5.319</b>
F-Clip@0.4	LBD	0.790	12.950	0.948	14.130	—	—
	DLD	0.306	5.321	0.944	13.025	67.799	153.450
	WLD	0.594	8.396	1.599	25.394	3.114	71.209
	LineTR	0.061	1.579	<u>0.074</u>	<u>1.517</u>	—	—
	SOLD2	0.095	2.164	0.295	3.968	<u>0.431</u>	<u>12.772</u>
HAWP@0.7	LBD	1.993	34.954	2.050	32.943	—	—
	DLD	1.462	23.861	1.904	27.084	—	—
	WLD	1.533	25.016	2.425	44.257	—	—
	LineTR	<u>0.058</u>	1.602	0.079	1.521	—	—
	SOLD2	<u>0.058</u>	<u>1.383</u>	0.356	4.202	0.517	16.713

HAWP. The ground truth poses are obtained by transforming the absolute poses provided by the authors of the original datasets. Then estimated pose is compared with ground truth pose and classical Relative Pose Error (RPE) is calculated for rotation ( $\epsilon_{rot}$ ) and translation ( $\epsilon_{trans}$ ).

The results are presented in table VIII. It can be seen that the LSD + LineTR combination shows superior results on all datasets except fr3/cabinet. Also, the results of association SOLD2 and LineTR with all three detectors are superior to the rest of the considered detector-association combinations. The reason why LSD produces good results, probably, as in the case of repeatability metrics, is better line reprojection.

### E. Performance

In addition to evaluating the quality of detectors and associations, we evaluate their performance. We measure the speed of work on all datasets. For all neural networks, we set the batch size to 1. It is important to note that we compare all the algorithms using python code so that the results may differ from the original implementations. It is also worth considering that we run LSDNet on CPU since the authors provided such a version of the algorithm. The results obtained are presented in tables II, III and VII. It is easy to see that handcrafted detectors, for example, EDLines and FLD, significantly outperform neural network algorithms regarding speed. However, it should be noted that there

are quite fast algorithms among neural network detectors, for example, M-LSD. Neural network association, in turn, significantly loses to LBD in terms of speed.

## VI. CONCLUSION

In this paper, we have presented a complete and exhaustive comparison for using visual lines in a SLAM front-end. To do so, we have labeled popular SLAM sequences from ICL NUIM and TUM RGB-D datasets. In particular, we have provided 17 line detection algorithms, 5 line associations methods and the resultant pose error or aligning a pair of frames with several combinations of detector-association. These results are the solid ground from which to benchmark the visual SLAM front-end involving lines, in all its stages: from detection to its effect in pose error.

## REFERENCES

- [1] R. Gomez-Ojeda, F.-A. Moreno, D. Zuniga-Noël, D. Scaramuzza, and J. Gonzalez-Jimenez, "PI-slam: A stereo slam system through the combination of points and line segments," *IEEE Transactions on Robotics*, vol. 35, no. 3, pp. 734–746, 2019.
- [2] Y. Li, R. Yunus, N. Brasch, N. Navab, and F. Tombari, "Rbg-d slam with structural regularities," in *2021 IEEE International Conference on Robotics and Automation (ICRA)*. IEEE, 2021, pp. 11 581–11 587.
- [3] A. Pumarola, A. Vakhitov, A. Agudo, A. Sanfeliu, and F. Moreno-Noguer, "PI-slam: Real-time monocular visual slam with points and lines," in *2017 IEEE international conference on robotics and automation (ICRA)*. IEEE, 2017, pp. 4503–4508.
- [4] X. Zuo, X. Xie, Y. Liu, and G. Huang, "Robust visual slam with point and line features," in *2017 IEEE/RSJ International Conference on Intelligent Robots and Systems (IROS)*. IEEE, 2017, pp. 1775–1782.
- [5] Y. Liu, D. Yang, J. Li, Y. Gu, J. Pi, and X. Zhang, "Stereo visual-inertial slam with points and lines," *IEEE Access*, vol. 6, pp. 69 381–69 392, 2018.
- [6] R. Wang, K. Di, W. Wan, and Y. Wang, "Improved point-line feature based visual slam method for indoor scenes," *Sensors*, vol. 18, no. 10, p. 3559, 2018.
- [7] Q. Fu, H. Yu, L. Lai, J. Wang, X. Peng, W. Sun, and M. Sun, "A robust rgb-d slam system with points and lines for low texture indoor environments," *IEEE Sensors Journal*, vol. 19, no. 21, pp. 9908–9920, 2019.
- [8] S. J. Lee and S. S. Hwang, "Elaborate monocular point and line slam with robust initialization," in *Proceedings of the IEEE/CVF International Conference on Computer Vision*, 2019, pp. 1121–1129.
- [9] Y. Li, N. Brasch, Y. Wang, N. Navab, and F. Tombari, "Structure-slam: Low-drift monocular slam in indoor environments," *IEEE Robotics and Automation Letters*, vol. 5, no. 4, pp. 6583–6590, 2020.
- [10] J. Lee and S.-Y. Park, "PIF-vins: Real-time monocular visual-inertial slam with point-line fusion and parallel-line fusion," *IEEE Robotics and Automation Letters*, vol. 6, no. 4, pp. 7033–7040, 2021.
- [11] R. Yunus, Y. Li, and F. Tombari, "Manhattanslam: Robust planar tracking and mapping leveraging mixture of manhattan frames," in *2021 IEEE International Conference on Robotics and Automation (ICRA)*. IEEE, 2021, pp. 6687–6693.
- [12] F. Shu, J. Wang, A. Pagani, and D. Stricker, "Structure plp-slam: Efficient sparse mapping and localization using point, line and plane for monocular, rgb-d and stereo cameras," *arXiv preprint arXiv:2207.06058*, 2022.
- [13] R. G. Von Gioi, J. Jakubowicz, J.-M. Morel, and G. Randall, "Lsd: A fast line segment detector with a false detection control," *IEEE transactions on pattern analysis and machine intelligence*, vol. 32, no. 4, pp. 722–732, 2008.
- [14] L. Zhang and R. Koch, "An efficient and robust line segment matching approach based on lbd descriptor and pairwise geometric consistency," *Journal of visual communication and image representation*, vol. 24, no. 7, pp. 794–805, 2013.
- [15] C. Akinlar and C. Topal, "Edlines: A real-time line segment detector with a false detection control," *Pattern Recognition Letters*, vol. 32, no. 13, pp. 1633–1642, 2011.
- [16] J. H. Lee, S. Lee, G. Zhang, J. Lim, W. K. Chung, and I. H. Suh, "Outdoor place recognition in urban environments using straight lines," in *2014 IEEE International Conference on Robotics and Automation (ICRA)*. IEEE, 2014, pp. 5550–5557.
- [17] E. J. Almazan, R. Tal, Y. Qian, and J. H. Elder, "Mcmlsd: A dynamic programming approach to line segment detection," in *Proceedings of the IEEE Conference on Computer Vision and Pattern Recognition*, 2017, pp. 2031–2039.
- [18] I. Suárez, E. Muñoz, J. M. Buenaposada, and L. Baumela, "Fsg: A statistical approach to line detection via fast segments grouping," in *2018 IEEE/RSJ International Conference on Intelligent Robots and Systems (IROS)*. IEEE, 2018, pp. 97–102.
- [19] I. Suárez, J. M. Buenaposada, and L. Baumela, "Elsed: Enhanced line segment drawing," *Pattern Recognition*, vol. 127, p. 108619, 2022.

- [20] K. Huang, Y. Wang, Z. Zhou, T. Ding, S. Gao, and Y. Ma, "Learning to parse wireframes in images of man-made environments," in *Proceedings of the IEEE Conference on Computer Vision and Pattern Recognition*, 2018, pp. 626–635.
- [21] N. Xue, S. Bai, F. Wang, G.-S. Xia, T. Wu, and L. Zhang, "Learning attraction field representation for robust line segment detection," in *Proceedings of the IEEE/CVF Conference on Computer Vision and Pattern Recognition*, 2019, pp. 1595–1603.
- [22] Y. Zhou, H. Qi, and Y. Ma, "End-to-end wireframe parsing," in *Proceedings of the IEEE/CVF International Conference on Computer Vision*, 2019, pp. 962–971.
- [23] Z. Zhang, Z. Li, N. Bi, J. Zheng, J. Wang, K. Huang, W. Luo, Y. Xu, and S. Gao, "Ppgnet: Learning point-pair graph for line segment detection," in *Proceedings of the IEEE/CVF Conference on Computer Vision and Pattern Recognition*, 2019, pp. 7105–7114.
- [24] Y. Lin, S. L. Pinteá, and J. C. van Gemert, "Deep hough-transform line priors," in *Computer Vision–ECCV 2020: 16th European Conference, Glasgow, UK, August 23–28, 2020, Proceedings, Part XXII 16*. Springer, 2020, pp. 323–340.
- [25] S. Huang, F. Qin, P. Xiong, N. Ding, Y. He, and X. Liu, "Tp-lsd: tri-points based line segment detector," in *Computer Vision–ECCV 2020: 16th European Conference, Glasgow, UK, August 23–28, 2020, Proceedings, Part XXVII 16*. Springer, 2020, pp. 770–785.
- [26] N. Xue, T. Wu, S. Bai, F. Wang, G.-S. Xia, L. Zhang, and P. H. Torr, "Holistically-attracted wireframe parsing," in *Proceedings of the IEEE/CVF Conference on Computer Vision and Pattern Recognition*, 2020, pp. 2788–2797.
- [27] Y. Xu, W. Xu, D. Cheung, and Z. Tu, "Line segment detection using transformers without edges," in *Proceedings of the IEEE/CVF Conference on Computer Vision and Pattern Recognition*, 2021, pp. 4257–4266.
- [28] G. Gu, B. Ko, S. Go, S.-H. Lee, J. Lee, and M. Shin, "Towards real-time and light-weight line segment detection," *arXiv preprint arXiv:2106.00186*, 2021.
- [29] H. Li, H. Yu, J. Wang, W. Yang, L. Yu, and S. Scherer, "Ulsd: Unified line segment detection across pinhole, fisheye, and spherical cameras," *ISPRS Journal of Photogrammetry and Remote Sensing*, vol. 178, pp. 187–202, 2021.
- [30] L. Teplyakov, L. Erlygin, and E. Shvets, "Lsdnet: Trainable modification of lsd algorithm for real-time line segment detection," *IEEE Access*, vol. 10, pp. 45 256–45 265, 2022.
- [31] X. Dai, H. Gong, S. Wu, X. Yuan, and M. Yi, "Fully convolutional line parsing," *Neurocomputing*, vol. 506, pp. 1–11, 2022.
- [32] K. Li, J. Yao, and X. Lu, "Robust line matching based on ray-point-ray structure descriptor," in *Computer Vision-ACCV 2014 Workshops: Singapore, Singapore, November 1–2, 2014, Revised Selected Papers, Part I 12*. Springer, 2015, pp. 554–569.
- [33] K. Li, J. Yao, X. Lu, L. Li, and Z. Zhang, "Hierarchical line matching based on line-junction-line structure descriptor and local homography estimation," *Neurocomputing*, vol. 184, pp. 207–220, 2016.
- [34] Q. Jia, X. Gao, X. Fan, Z. Luo, H. Li, and Z. Chen, "Novel coplanar line-points invariants for robust line matching across views," in *Computer Vision–ECCV 2016: 14th European Conference, Amsterdam, The Netherlands, October 11–14, 2016, Proceedings, Part VIII 14*. Springer, 2016, pp. 599–611.
- [35] A. Vakhitov and V. Lempitsky, "Learnable line segment descriptor for visual slam," *IEEE Access*, vol. 7, pp. 39 923–39 934, 2019.
- [36] M. Lange, F. Schweinfurth, and A. Schilling, "Dld: A deep learning based line descriptor for line feature matching," in *2019 IEEE/RSJ International Conference on Intelligent Robots and Systems (IROS)*. IEEE, 2019, pp. 5910–5915.
- [37] M. Lange, C. Raisch, and A. Schilling, "Wld: A wavelet and learning based line descriptor for line feature matching," 2020.
- [38] Q. Ma, G. Jiang, and D. Lai, "Robust line segments matching via graph convolution networks," *arXiv preprint arXiv:2004.04993*, 2020.
- [39] M. Chen, S. Yan, R. Qin, X. Zhao, T. Fang, Q. Zhu, and X. Ge, "Hierarchical line segment matching for wide-baseline images via exploiting viewpoint robust local structure and geometric constraints," *ISPRS Journal of Photogrammetry and Remote Sensing*, vol. 181, pp. 48–66, 2021.
- [40] S. Yoon and A. Kim, "Line as a visual sentence: Context-aware line descriptor for visual localization," *IEEE Robotics and Automation Letters*, vol. 6, no. 4, pp. 8726–8733, 2021.
- [41] C. Qiao, T. Bai, Z. Xiang, Q. Qian, and Y. Bi, "Superline: A robust line segment feature for visual slam," in *2021 IEEE/RSJ International Conference on Intelligent Robots and Systems (IROS)*. IEEE, 2021, pp. 5664–5670.
- [42] P. Rahmdel, R. A. Comley, D. Shi, and S. McElduff, "A review of hough transform and line segment detection approaches," 2015.
- [43] J. Illingworth and J. Kittler, "A survey of the hough transform," *Computer vision, graphics, and image processing*, vol. 44, no. 1, pp. 87–116, 1988.
- [44] R. O. Duda and P. E. Hart, "Use of the hough transformation to detect lines and curves in pictures," *Communications of the ACM*, vol. 15, no. 1, pp. 11–15, 1972.
- [45] R. S. Stephens, "Probabilistic approach to the hough transform," *Image and vision computing*, vol. 9, no. 1, pp. 66–71, 1991.
- [46] J. Matas, C. Galambos, and J. Kittler, "Robust detection of lines using the progressive probabilistic hough transform," *Computer vision and image understanding*, vol. 78, no. 1, pp. 119–137, 2000.
- [47] L. A. Fernandes and M. M. Oliveira, "Real-time line detection through an improved hough transform voting scheme," *Pattern recognition*, vol. 41, no. 1, pp. 299–314, 2008.
- [48] Y. Furukawa and Y. Shinagawa, "Accurate and robust line segment extraction by analyzing distribution around peaks in hough space," *Computer vision and image understanding*, vol. 92, no. 1, pp. 1–25, 2003.
- [49] J. B. Burns, A. R. Hanson, and E. M. Riseman, "Extracting straight lines," *IEEE transactions on pattern analysis and machine intelligence*, no. 4, pp. 425–455, 1986.
- [50] M. Boldt, R. Weiss, and E. Riseman, "Token-based extraction of straight lines," *IEEE Transactions on Systems, Man, and Cybernetics*, vol. 19, no. 6, pp. 1581–1594, 1989.
- [51] J. Song and M. R. Lyu, "A hough transform based line recognition method utilizing both parameter space and image space," *Pattern recognition*, vol. 38, no. 4, pp. 539–552, 2005.
- [52] A. Bandera, J. M. Pérez-Lorenzo, J. P. Bandera, and F. Sandoval, "Mean shift based clustering of hough domain for fast line segment detection," *Pattern Recognition Letters*, vol. 27, no. 6, pp. 578–586, 2006.
- [53] K. Li, J. Yao, M. Lu, Y. Heng, T. Wu, and Y. Li, "Line segment matching: A benchmark," in *2016 IEEE Winter Conference on Applications of Computer Vision (WACV)*. IEEE, 2016, pp. 1–9.
- [54] G. Medioni and R. Nevatia, "Segment-based stereo matching," *Computer vision, graphics, and image processing*, vol. 31, no. 1, pp. 2–18, 1985.
- [55] C. Schmid and A. Zisserman, "Automatic line matching across views," in *Proceedings of IEEE Computer Society Conference on Computer Vision and Pattern Recognition*. IEEE, 1997, pp. 666–671.
- [56] H. Bay, V. Ferraris, and L. Van Gool, "Wide-baseline stereo matching with line segments," in *2005 IEEE Computer Society Conference on Computer Vision and Pattern Recognition (CVPR'05)*, vol. 1. IEEE, 2005, pp. 329–336.
- [57] Z. Wang, F. Wu, and Z. Hu, "Mslsd: A robust descriptor for line matching," *Pattern Recognition*, vol. 42, no. 5, pp. 941–953, 2009.
- [58] H. Kim and S. Lee, "A novel line matching method based on intersection context," in *2010 IEEE International Conference on Robotics and Automation*. IEEE, 2010, pp. 1014–1021.
- [59] B. Fan, F. Wu, and Z. Hu, "Robust line matching through line-point invariants," *Pattern Recognition*, vol. 45, no. 2, pp. 794–805, 2012.
- [60] L. Wang, U. Neumann, and S. You, "Wide-baseline image matching using line signatures," in *2009 IEEE 12th International Conference on Computer Vision*. IEEE, 2009, pp. 1311–1318.
- [61] R. Pautrat, J.-T. Lin, V. Larsson, M. R. Oswald, and M. Pollefeys, "Sold2: Self-supervised occlusion-aware line description and detection," in *Proceedings of the IEEE/CVF Conference on Computer Vision and Pattern Recognition*, 2021, pp. 11 368–11 378.
- [62] G. Zhang, J. H. Lee, J. Lim, and I. H. Suh, "Building a 3-d line-based map using stereo slam," *IEEE Transactions on Robotics*, vol. 31, no. 6, pp. 1364–1377, 2015.
- [63] T.-j. Lee, C.-h. Kim, and D.-i. Do, "A monocular visual sensor-based efficient slam method for indoor service robots," *IEEE Transactions on Industrial Electronics*, vol. 66, no. 1, pp. 318–328, 2018.
- [64] Q. Fu, J. Wang, H. Yu, I. Ali, F. Guo, Y. He, and H. Zhang, "Pl-vins: Real-time monocular visual-inertial slam with point and line features," *arXiv preprint arXiv:2009.07462*, 2020.
- [65] P. Denis, J. H. Elder, and F. J. Estrada, "Efficient edge-based methods for estimating manhattan frames in urban imagery," in *Computer Vision–ECCV 2008: 10th European Conference on Computer Vision, Marseille, France, October 12–18, 2008, Proceedings, Part II 10*. Springer, 2008, pp. 197–210.
- [66] D. R. Martin, C. C. Fowlkes, and J. Malik, "Learning to detect natural image boundaries using local brightness, color, and texture cues," *IEEE transactions on pattern analysis and machine intelligence*, vol. 26, no. 5, pp. 530–549, 2004.
- [67] A. Handa, T. Whelan, J. McDonald, and A. J. Davison, "A benchmark for rgb-d visual odometry, 3d reconstruction and slam," in *2014 IEEE international conference on Robotics and automation (ICRA)*. IEEE, 2014, pp. 1524–1531.
- [68] J. Sturm, N. Engelhard, F. Endres, W. Burgard, and D. Cremers, "A benchmark for the evaluation of rgb-d slam systems," in *2012 IEEE/RSJ international conference on intelligent robots and systems*. IEEE, 2012, pp. 573–580.
- [69] A. Kornilova, D. Iarosh, D. Kukushkin, N. Goncharov, P. Mokeev, A. Saliou, and G. Ferrer, "Evops benchmark: Evaluation of plane segmentation from rgbd and lidar data," in *2022 IEEE/RSJ International Conference on Intelligent Robots and Systems (IROS)*. IEEE, 2022, pp. 13 074–13 080.
- [70] B. Sekachev et al., "opencv/cvat: v1.1.0." Aug. 2020. [Online]. Available: <https://doi.org/10.5281/zenodo.4009388>
- [71] K. M. Yi, E. Trulls, Y. Ono, V. Lepetit, M. Salzmann, and P. Fua, "Learning to find good correspondences," in *Proceedings of the IEEE conference on computer vision and pattern recognition*, 2018, pp. 2666–2674.
- [72] P.-E. Sarlin, D. DeTone, T. Malisiewicz, and A. Rabinovich, "Superglue: Learning feature matching with graph neural networks," in *Proceedings of the IEEE/CVF conference on computer vision and pattern recognition*, 2020, pp. 4938–4947.
- [73] R. Kümmerle, G. Grisetti, H. Strasdat, K. Konolige, and W. Burgard, "g 2 o: A general framework for graph optimization," in *2011 IEEE International Conference on Robotics and Automation*. IEEE, 2011, pp. 3607–3613.
- [74] M. Nieto, C. Cuevas, L. Salgado, and N. García, "Line segment detection using weighted mean shift procedures on a 2d slice sampling strategy," *Pattern Analysis and Applications*, vol. 14, pp. 149–163, 2011.